Yassine Dahbi, 2025, 13:4
ISSN (Online): 2348-4098
ISSN (Print): 2395-4752

International Journal of Science, Engineering and Technology

An Open Access Journal

Fracture Mechanisms of Laminated Bamboo under Four-Point Bending with Varying Lay-Up Configurations and Notch Ratios Supported by SEM Observations

Yassine Dahbi, Yao Wu, Huang Xuejian, Hamza Zaouri,
College of Civil Engineering, Nanjing Tech University, 30 South Puzhu Road, Nanjing 211816, Jiangsu Province, China

Abstract- This study investigates the mechanical properties of laminated bamboo composites through four-point shear bending tests. Eight groups were prepared with various lay-up configurations and two notches with different initial notch-to-depth ratios to assess the effect of notch size and fibre orientation on fracture behaviour. The test programme was designed to examine the fracture process, specifically focusing on crack initiation, crack growth, and ultimate failure, while also recording load–CMOD, load–displacement, and load–CMSD responses. Fracture surfaces after the test will also be investigated by scanning electron microscopy (SEM) to provide microstructural data on crack mechanisms and modes of failure. From comparison of the results of all configurations, the research identifies the best lay-up design in terms of strength, toughness, and energy absorption. Such data is extremely valuable for enhancing laminated bamboo structures from an engineering point of view.

Keywords: Laminated bamboo, Four-point bending, Fracture mechanic, Notch-to-depth ratio, Sustainable materials, Flexural behaviour, Crack propagation, SEM analysis.

I. INTRODUCTION

Sustainability and durability are emerging as the highest concerns in modern construction, with industries and researchers looking for renewable alternatives to traditional materials. Among them, laminated bamboo is a leading candidate, as it exhibits rapid growth and is environmentally friendly. It possesses excellent mechanical properties. Hardwoods take years to develop, but bamboo matures within 3–5 years, which is essentially an infinitely renewable material. In addition to its exceptionally rapid growth, bamboo absorbs substantial quantities of carbon dioxide, mitigating the effects of climate change and further strengthening its role as a green building material [1–4]. In addition to its environmental advantages, bamboo boasts a remarkable strength-to-weight ratio, traditionally comparable to or even superior to that of conventional hardwoods and metals. When laminated into composites, the fibres of bamboo are straightened and bonded in proximity to reduce natural heterogeneity and enhance uniformity, thereby ensuring mechanical strength for use in beams, panels, flooring, and even prefabricated buildings [5–10]. Lamination also enhances the resistance of bamboo to moisture, insects, and warping to make it an effective material for both traditional and modern applications. More work has been done on the mechanical properties of laminated bamboo, with excellent tensile,

compressive, flexural, and shear properties being reported. Experiments confirm that fibre orientation selection and the adhesive system are factors of primary importance. For example, 0/90/0 and 90/0/90 orientations had a significant effect on flexure, while cross-laminated configurations improve multipath loading shear strength [11–15].

Additionally, laminated bamboo is resistant to impact and dynamic loading, making it favourable in seismic regions [16, 17]. Yet, environmental sensitivity, particularly towards humidity and moisture, remains a concern for long-term stability [18]. Despite such progress, significant knowledge gaps remain. Particularly, there is limited understanding of how laminate layer interaction and initial notch-to-depth ratios influence fracture initiation, crack propagation, and total energy absorption. Additionally, fracture mechanisms such as delamination, fibre pull-out, and crack branching have not been thoroughly examined under various lay-up configurations. Addressing these gaps is crucial for optimising laminated bamboo as a high-performance structural material. Consequently, this study explores the fracture behaviour of five-layer laminated bamboo through four-point shear bending tests with two notch-to-depth ratios (0.5 and 0.6). Eight different lay-up orientations were fabricated to assess how notch depth and fibre orientation affect stiffness, strength, and fracture resistance. Mechanical testing is supplemented by scanning electron microscopy (SEM) to analyse microstructural failure modes and gain insights into crack development. By correlating structural performance with fracture morphology, this research aims to identify optimal configurations that balance strength, ductility, and fracture toughness, thereby providing valuable guidance for incorporating laminated bamboo into sustainable structural systems. [19–22].

II. EXPERIMENTS

In this study, two laminated bamboo panels were used for the experiments as shown in Figure 1, Each panel consisted of five layers. The bamboo strips were carbonised at 120°C to improve the material's stability and strength. Lamination was performed using urea-formaldehyde (UF) resin to bond the strips together. The panels measured 2000 mm × 1000 mm and consisted of bamboo strips with individual thicknesses of 5 mm, widths ranging from 20 to 25 mm, and lengths of about 2400 mm. These strips were aligned along the bamboo culm's longitudinal direction, in line with standard practices to enhance the strength properties of laminated bamboo. For the Cross-Laminated Bamboo (CLB) panels used in this study, two initial depth ratios (a_0/D = 0.5 and 0.6) were tested to assess the influence of different configurations on mechanical properties.

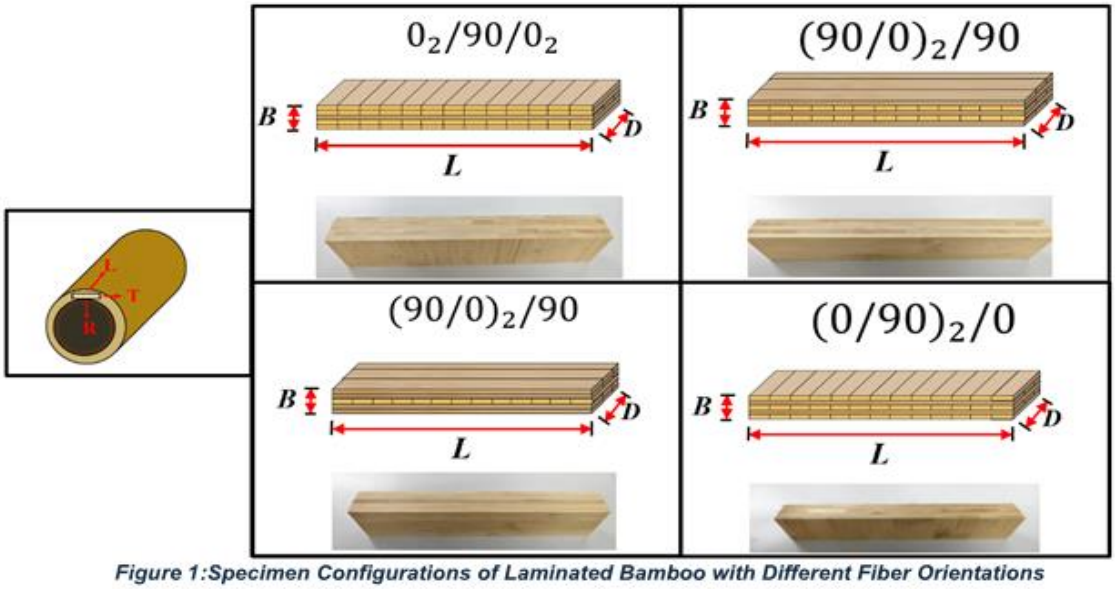

Figure 1:Specimen Configurations of Laminated Bamboo with Different Fiber Orientations

Each type of CLB panel was hot-pressed at a pressure of 3 MPa and a temperature of 105°C for 3 minutes to ensure proper bonding. The final oven-dry density of the laminated bamboo was measured at 0.0157 g/cm^3, with a standard deviation of 49.3 kg/m^3. Before testing, all specimens were conditioned for at least seven days in an environment maintained at 20 ± 0.5°C and 60 ± 2% humidity to achieve moisture equilibrium. The average moisture content, determined via electrical resistance measurement, was 8.17%. Specimens were labelled according to their lay-up configuration and notch-to-depth ratio (a_0/D). The two notch-to-depth ratios examined were 0.5 and 0.6, representing cuts of 50% and 60% of the depth (D), respectively. Notches were created using a 0.24 mm thick saw blade, with 10 specimens prepared for each configuration. The dimensions of the test specimens used for the transverse bending (TPB) fracture tests were 50 mm × 30 mm × 250 mm.

Testing setup

Four-point shear bending (FSB) tests were conducted on a universal testing machine to ensure stable and precise loading. Figure 2. The loading configuration consisted of two symmetrical loads: P1, applied at a distance c from the specimen centerline, and P2, applied at a distance l from the centerline. This arrangement generated a distinct shear zone between the loading points, which is suitable for investigating the combined bending–shear response of laminated bamboo. Observe that this support configuration may lead to errors in the calculation of fracture toughness due to frictional effects, as indicated in the literature [23, 24, 25]. Displacement at the supporting and loading points was recorded by mechanical displacement meters. Furthermore, the clip gauges were installed at the notch to record both crack mouth opening displacement (CMOD) and crack mouth slip displacement (CMSD).

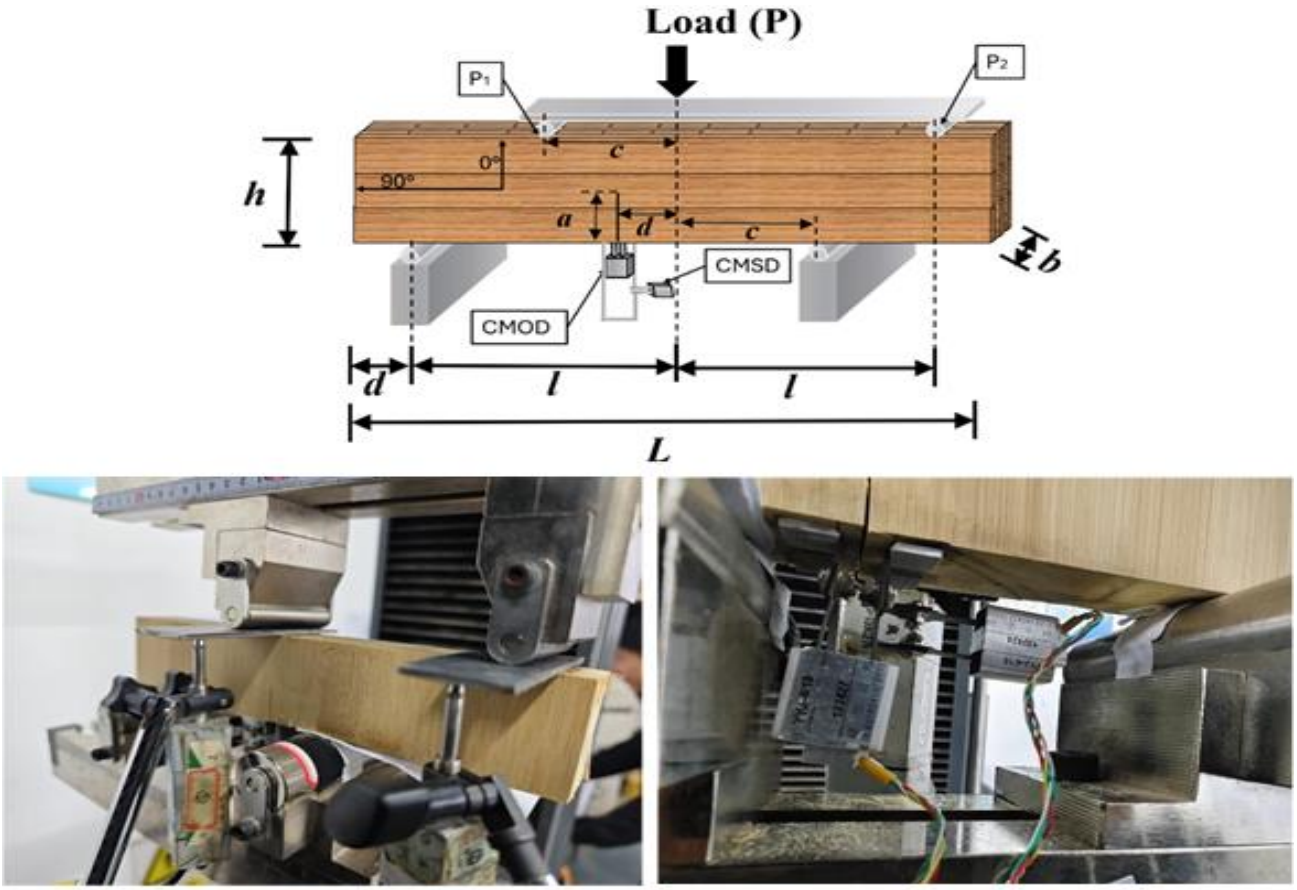

Figure 1:Four-Point Shear Bending Test Setup for Laminated Bamboo Specimens

All displacement and load data were obtained using a wireless static strain acquisition system, allowing for the real-time monitoring of crack initiation and propagation during the tests. The load was imposed in displacement control at 0.1 mm/min, and the force applied was monitored with a tension–compression load cell of 70 kN capacity [26, 27]. Initial crack length (a) was initiated at l–d, where l is the distance between the specimen centerline and the P2 loading point, and d is the distance between the centerline and the initial crack tip. Two notch-to-depth ratios (a/h = 0.5 and 0.6) were considered to study the effect of crack size on fracture properties. Table 1. The notches were cut using a 0.24 mm thickness saw blade for accuracy and uniformity among specimens [28, 29]. As the experimental data are inherently discrete, the data analysis process followed the approach given by Dong et al. [30]. From each group of specimens, 10 samples were prepared.

Table 1, and the P–CMOD curve closest to the group average was chosen to represent the fracture response of laminated bamboo, thereby reducing scatter and maintaining consistency. In addition, other standard characteristic curves were derived, including the P–δ curve, P–CMSD curve, P1–δ1 curve (where δ1 is the displacement at the inner loading point), and P2–δ2 curve (where δ2 is the displacement at the outer loading point). Based on these data sets, specific key fracture parameters were determined, including initial crack load, peak load, fracture toughness, and fracture energy [31, 32]. This elaborate setup and analysis procedure enabled a reliable determination of the flexural–shear behaviour and fracture process of five-layer laminated bamboo specimens, while also providing clear insight into the influence of notch-to-depth ratios (0.5 and 0.6) on layer interaction and crack propagation.

Table 1:Specimen Details: Dimensions, Lay-Up Configurations, and Initial Notch Ratios

specimens	L×b×h (mm)	a/h	c (mm)	d (mm)	l (mm)	a (mm)	Number of specimens
Grp 1: $0_2/90/0_2$	250×50×30	0.5	20	10	200	20	10
Grp 2: $0_2/90/0_2$	250×50×30	0.6	20	10	200	25	10
Grp 3: $90_2/0/90_2$	250×50×30	0.5	20	10	200	15	10
Grp 4: $90_2/0/90_2$	250×50×30	0.6	20	10	200	20	10
Grp 5: $(0/90)_2/0$	250×50×30	0.5	20	10	200	15	10
Grp 6: $(0/90)_2/0$	250×50×30	0.6	20	10	200	20	10
Grp7: $(90/0)_2/90$	250×50×30	0.5	20	10	200	15	10
Grp 8: $(90/0)_2/90$	250×50×30	0.6	20	10	200	20	10

To more effectively evaluate the mechanical performance of 0.5 and 0.6 initial depth ratio laminated bamboo, test data are represented by load–CMOD, load–displacement, and load–CMSD curves. These curves provide valuable information on crack initiation, propagation, shear sliding behaviour, and energy absorption capacity of the samples. By comparing the response of the various lay-up configurations on these graphs, one can determine the role of fibre orientation and notch depth on stiffness, ductility, and fracture toughness. The subsequent sections provide details on the results of each group and the variations in their structural behaviour.

Load-CMOD curves of 0.5 initial depth ratio specimens

The Load-CMOD curves for Grp 1 show a moderate load-carrying capacity with a peak load of around 8 kN Figure 3. With the maximum reached, the load is observed to drop suddenly while CMOD continues to increase, indicating brittle failure. Although there is some scatter among specimens, the overall trend suggests low toughness and early crack propagation. For Grp 3, the plots show that all 0.5 ratio groups exhibit maximum early stiffness and load resistance, with peak loads ranging from 10 to 20 kN. The high rate of load rise followed by sudden failure is typical of a brittle fracture mode. Still, the overall high levels of load throughout the specimens indicate signs of greater structural ability. This greater performance is due to the higher proportion of 90° layers, which enhances resistance to shear loading and bending by distributing the stresses across the laminate thickness. Group 3 thus appears to provide the best balance between stiffness and strength when the top priority is given to maximum load carrying ability. Grp 5 specimens show maximum loads of 12–16 kN with the post-peak drop being less abrupt than Grp 3. CMOD goes up to 7–8 mm, which is a testament to stable crack growth and higher fracture toughness. While Grp 5 is higher in energy absorption before failure, its maximum loads are slightly lower and non-uniform compared to Group 3. Finally, Grp 7 has ultimate loads between 10–15 kN. Ductile behaviour is exhibited by the curves with longer CMOD values greater than 6 mm, indicating a higher tolerance to deformation. This makes Grp 7 suitable to be utilised in situations where maximum stiffness is less critical compared to energy absorption and ductility. Overall, Grp 3 is identified as the best configuration of the 0.5 ratio groups, probably due to its higher ratio of 90° layers that contribute to higher stiffness and load-carrying ability.

Load-Displacement curves of 0.5 initial depth ratio specimens

The Load-Displacement curves Figure 4 of the groups initiating with a depth ratio of 0.5 show apparent variations in ductility and strength. Group 1 shows a sharp rise to around 8 kN, followed by an abrupt loss and a steady fall, with displacements up to 14–16 mm, indicating brittle-like fracture and negligible energy absorption. On the other hand, Grp 3 supports the highest peak loads of 18–22 kN and maintains strength at a wide displacement range of 25–30 mm with higher stiffness, load capacity, and energy absorption. Grp 5 develops maximum loads of 12–16 kN and deforms to 15–20 mm before failure, indicating a confluence of strength and ductility with greater variation than Grp 3. Finally, Grp 7 peeks at 12–15 kN with 15–20 mm displacements, combining intermediate strength with added flexibility and energy absorption but with less consistency between specimens. Overall, the comparison indicates Grp 3 as being the most performing of all configurations since it comprises a higher percentage of the stiffest and load-carrying 90° layers that support the most significant loads over the most extensive displacement range.

Load-CMSD curves of 0.5 initial depth ratio specimens

Load-CMSD curves Figure 4 for the 0.5 series are seen to exhibit apparent differences in the shear displacement capacity and mode of failure. Grp 1 experienced peak loads of around 8 kN but failed at extremely low CMSD, generally less than 2 mm, indicating a brittle shear mode of failure with little sliding capacity. In contrast, Grp 3 resisted the maximum loads, 18–22 kN, and remained difficult for CMSD up to 12 mm with enhanced shear sliding resistance and high shear toughness. Grp 5 withstood loads of 12–16 kN with CMSD up to 8–10 mm, with similar load capacity and shear

displacement performance but with higher variability than Grp 3. Similarly, Grp 7 withstood maximum loads of 12–15 kN and CMSD up to 8–10 mm, with stable crack formation and high shear strength, but again less consistently than Grp 3. Overall, comparison makes Grp 3 the best performing group in shear resistance owing to its higher proportion of 90° layers, which have been shown to achieve higher load capacity as well as the ability to resist higher shear displacements before failure.

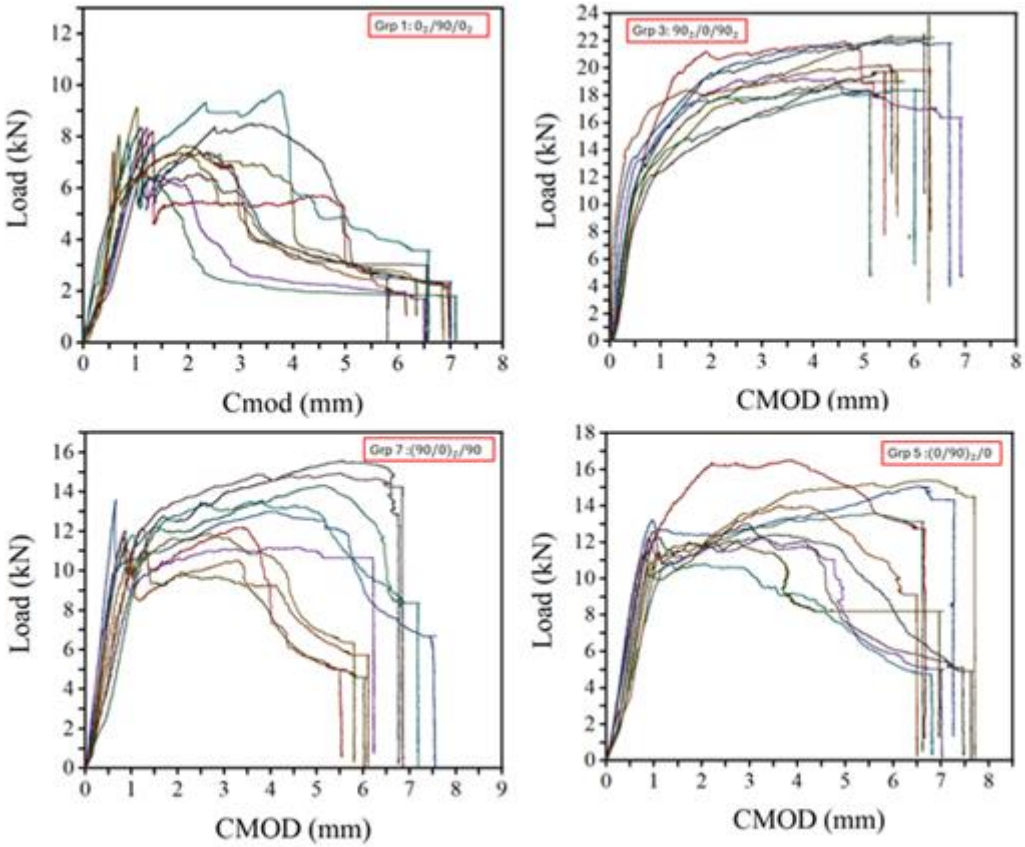

Figure 1:Load-CMOD curves of grp1,3,5,7

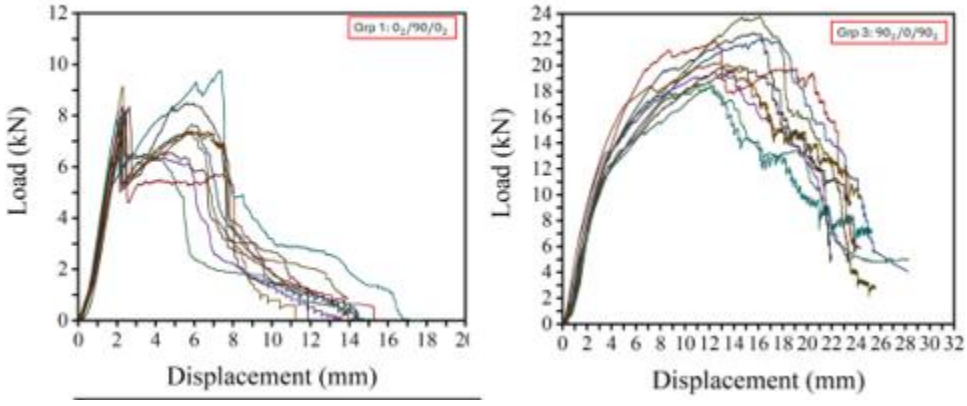

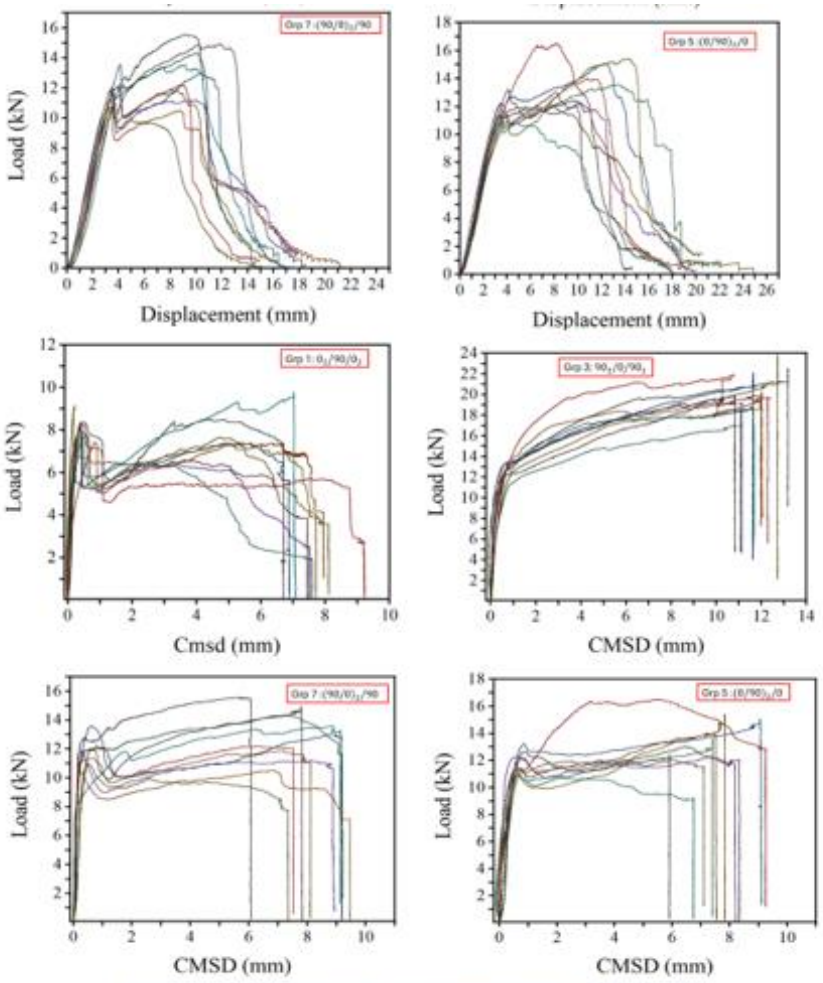

Figure 4:Load-displacement, Load-CMSD curves of grp 1,3,5,7

Load-CMOD curves of 0.6 initial depth ratio specimens

Load-CMOD curves Figure 5 The depth ratio groups of 0.6 demonstrate a clear contrast in resistance to crack opening and fracture toughness. Grp 2 (0_2/90/0_2) could only carry peak loads of 7–8 kN before these fell sharply with increasing CMOD, with crack openings rarely exceeding 3–4 mm, indicating a brittle fracture mode with very low energy absorption. In comparison with Grp 4, it achieved much larger loads between 12–15 kN, with strength maintained over a broader range of CMOD (5–7 mm), indicating higher fracture toughness due to a greater number of 90° layers. Grp 6 exhibited intermediate performance, with maximum loads of 10–13 kN and CMOD values up to 6–7 mm. However, in some specimens, abrupt failure was noticed; others exhibited smoother reduction, showing intermittent resistance to crack development. In addition, Grp 8 developed 10–12 kN with CMOD to 6–7 mm, which showed good ductility and energy absorption but with low load carrying capacity compared to Grp 4. Overall, among the 0.6 groups, Grp 4 was found to be best, where high peak load capacity was accompanied by large CMOD values, stressing the beneficial effect of 90° orientations in fracture toughness as well as resisting crack growth.

Load-Displacement curves of 0.6 initial depth ratio specimens

The Load vs. Displacement curves Figure 6 Of the 0.6 initial depth ratio groups, some exhibit stark differences in ductility and strength. grp 2 reached maximum loads of about 7–8 kN at relatively small displacements of 6–10 mm, after which a sharp drop occurred, with brittle fracture and minimal energy absorption. In contrast, Grp 4 performed better, with maximum loads of 13–16 kN and displacements of 12–18 mm, followed by step-wise softening, which indicates superior toughness and energy absorption.

Group 6 achieved maximum loads of 10–13 kN with displacements of 15–18 mm, exhibiting comparable strength and ductility, but with variability in fracture mode between samples. Similarly, Grp 8 reached maximum loads of 11–13 kN and exhibited high displacements of 15–20 mm, suggesting moderate strength but greater ductility and energy absorption. Overall, among the 0.6 ratio groups, Grp 4 stands out because it combines high load capacity with high displacement tolerance and is thus considered the most structurally advantageous.

Load-CMSD curves of 0.6 initial depth ratio specimens

Load against CMSD Figure 6Values of 0.6 ratio groups indicate apparent differences in sliding capacity and shear resistance. Grp 2 exhibited maximum loads around 7–8 kN but exhibited non-unstable shear propagation with abrupt load drops, registering moderate energy absorption despite CMSD values of up to 7–8 mm. On the other hand, Grp 4 showed peak performance, sustaining 13–16 kN loads stably for similar CMSD ranges, with excellent shear toughness due to its high 90 ° layer content. Grp 6 showed mid-range performance, with 10–13 kN loads and CMSD up to 7–8 mm, though the scatter between the specimens indicated

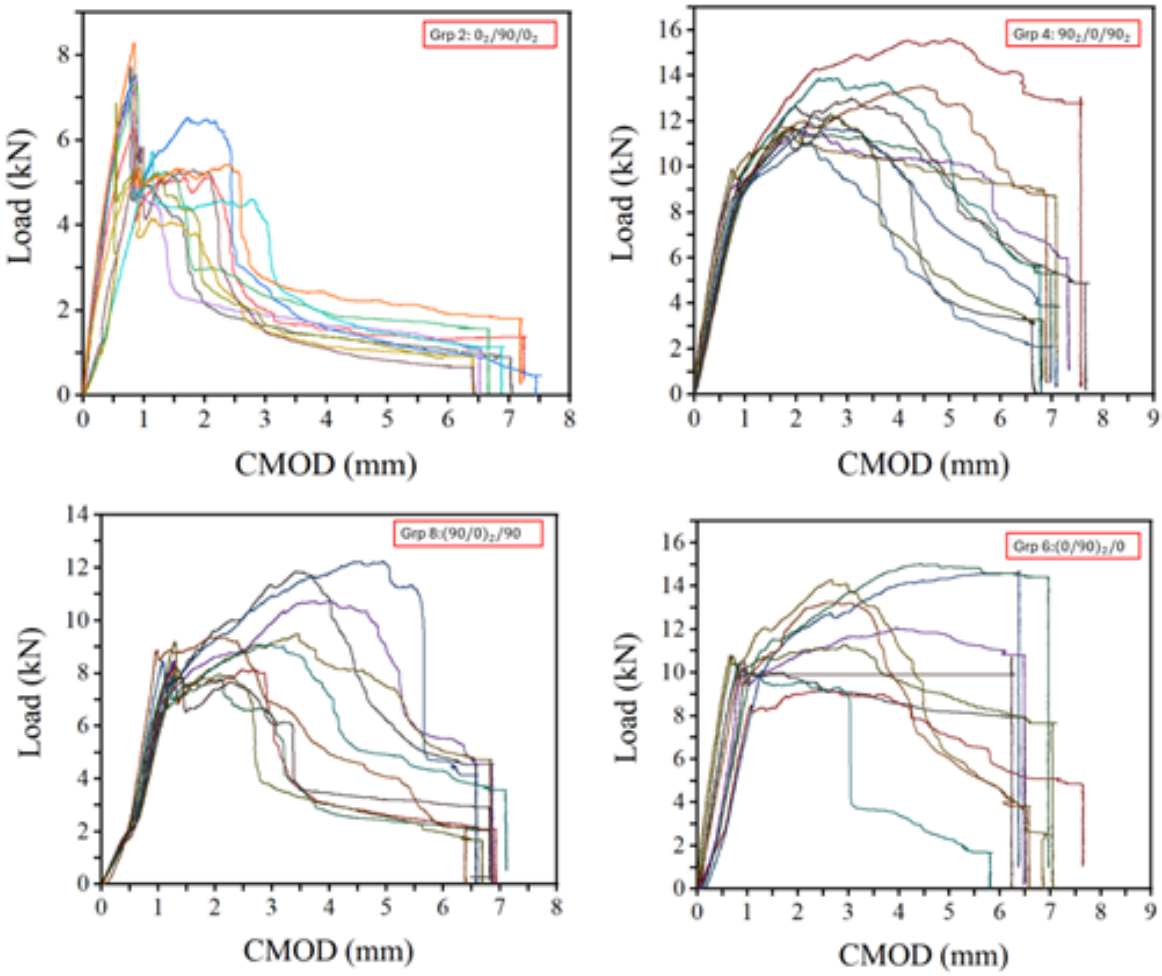

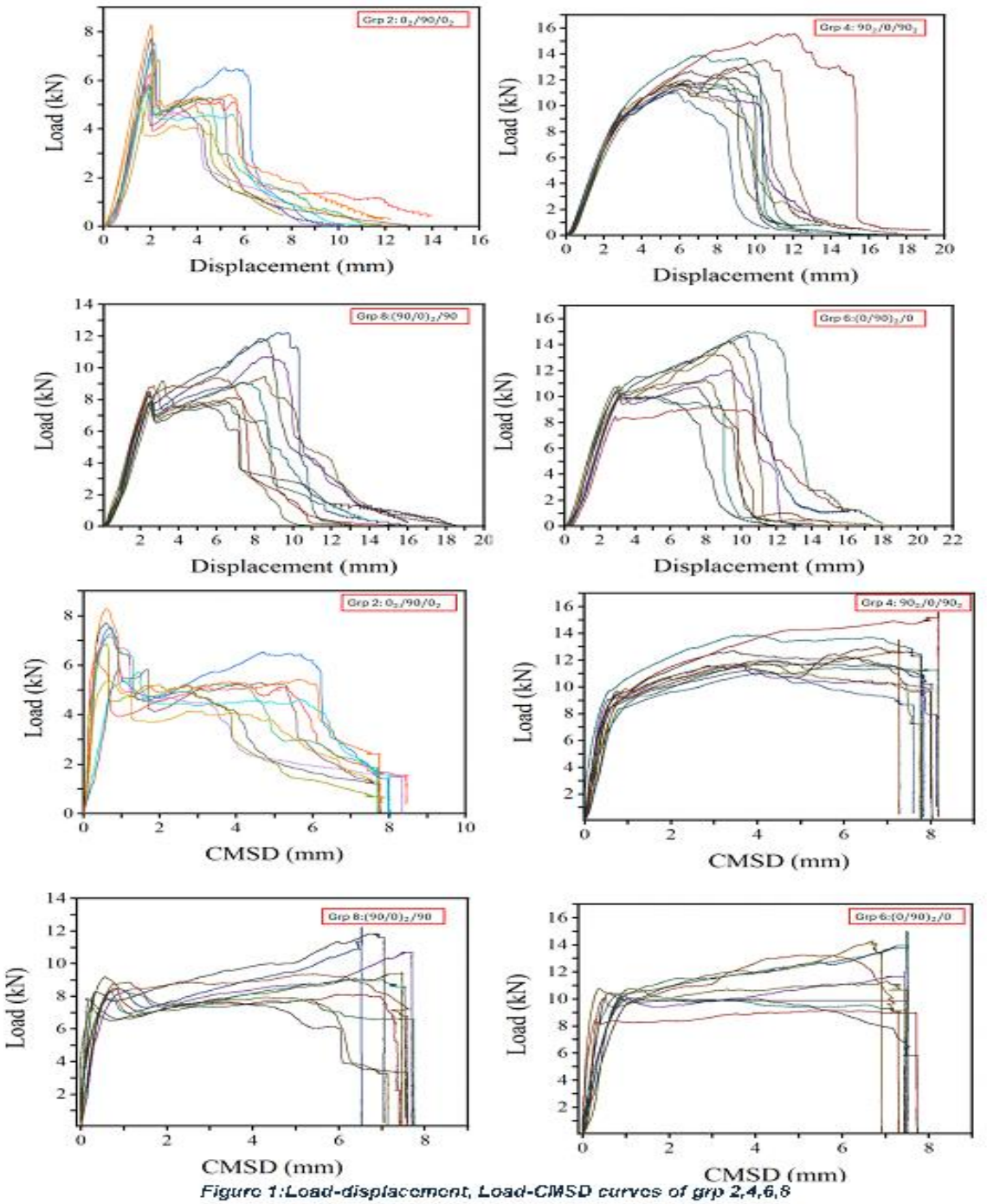

Figure 1:Load-displacement, Load-CMSD curves of grp 2,4,6,8

Lower reliability. Similarly, Group 8 also recorded 11–13 kN loads with stable shear displacement of 7–8 mm, resulting in a reasonable balance of ductility and moderate load-carrying capacity. In general, for the case of 0.6 ratio groups, Group 4 again proved to be the best configuration, producing the highest load-carrying capacity as well as stable shear resistance.

III. FRACTURE PROCESS

The fracture process was analysed in detail using one representative specimen from each group. The analysis presented here focuses on a single sample that closely reflects the average behaviour; only the groups with an initial notch-to-depth ratio of 0.5 are

examined in terms of their fracture evolution. This approach allows for a clearer understanding of crack initiation, propagation, and final failure while avoiding unnecessary repetition across all specimens.

Fracture Stages of Group 1 ($0_2/90/0_2$, a/h = 0.5)

In the initial phase Figure 7,Table 2At approximately 176 seconds under a load of 4.02 kN, an initial crack was observed at the notch tip, approximately 5.8 mm in length. Slight splitting sounds were heard, with the displacement, CMOD, and CMSD measured as 1.46 mm, 0.799 mm, and 0.25 mm, respectively. This was the initiation of elastic–plastic behaviour from the purely elastic one. During the second stage, at ~286 seconds and 7.43 kN, crack growth increased, reaching a size of ~9 mm, accompanied by a secondary branch of about 6 mm. Cracking was more audible, while displacement, CMOD, and CMSD reached about 2.38 mm, 1.396 mm, and 0.725 mm, respectively. The stage was representative of slow fibre–matrix debonding under load. In the third stage, at 308 seconds and a load of 4.89 kN, the crack length had reached about 10 mm. The top half of the specimen began to move by about 1.5 mm. Few weak splitting sounds were heard, and values for displacement, CMOD, and CMSD were 2.56 mm, 1.443 mm, and 1.456 mm. This stage was characterised by steady crack growth with partial delamination between layers. The fourth stage at approximately 621 seconds and a load of 8.97 kN was typified by greater propagation. The upper surface of the specimen had fallen by around 4 mm, and the width of the primary crack had increased significantly. Displacement, CMOD, and CMSD had also achieved 5.17 mm, 3.057 mm, and 4.019 mm, respectively. Shear sliding between layers increasingly controls fracture behaviour. In the fifth stage, at 788 seconds and 8.72 kN, the crack opening increased to nearly 6 mm with extensive delamination on the sample's left side. Displacement was 6.56 mm, CMOD was 3.852 mm, and CMSD was 5.86 mm. This was a stage of pre-failure instability because the bamboo layers showed unstable sliding and separation of cohesion. Finally, at the sixth stage, at 1233 seconds with a load of 8.87 kN, failure was catastrophic. The crack extended to approximately 12 mm, and the left half of the specimen dropped significantly. Displacement, CMOD, and CMSD increased substantially to 10.27 mm, 6.91 mm, and 7.09 mm. This stage was characterised by sudden bursting, fibre fracture, delamination, and complete loss of load-carrying capacity. Overall, the $0_2/90/0_2$ configuration exhibited a progressive fracture mechanism involving controlled crack extension at the initial stages, followed by shear-driven delamination, resulting in catastrophic failure via fibre breaking and sliding of the laminated layers.

Table 2:Fracture Stages of Group 1 ($0_2/90/0_2$, a/h = 0.5)

Stage	Time (s)	Load (kN)	Displacement (mm)	CMOD (mm)	CMSD (mm)	Crack Length (mm)
Stage 1	176	4.02	1.46	0.799	0.25	5.8
Stage 2	286	7.43	2.38	1.396	0.725	9 (+6 branch)
Stage 3	308	4.89	2.56	1.443	1.456	10 (+1.5 top shift)
Stage 4	621	8.97	5.17	3.057	4.019	9 (+4 opening)
Stage 5	788	8.72	6.56	3.852	5.86	6 (delamination)
Stage 6	1233	8.87	10.27	6.91	7.09	12

Fracture process for Group 3 ($90_2/0/90_2$, a/h = 0.5)

The cracking process of Group 3 Table 3,Figure 8specimens experienced six stages. During the early stage (196s, 6.48 kN), no visible change occurred, and the specimen remained intact under load. At 409 s, when the load had reached 11.41 kN, the earliest fine cracks formed and propagated horizontally to a distance of approximately 8.5 mm, with noticeable CMOD and CMSD increments. At 797 s and 14.72 kN, the crack lengthened by approximately 18 mm in horizontal growth, with a displacement of 6.64 mm and CMSD exhibiting a sudden rise. At 1446 s, the specimen reached its peak load of 18.06 kN, where an inclined upward crack was observed in the area of the loading point, and significant displacement occurred (12.05 mm), marking the beginning of unstable fracture. By 1718 s, the load reduced to 15.89 kN, and the initial crack extended downwards by around 12.5 mm, while a secondary crack formed

near the loading point (~9 mm). Finally, at 1961 s, at 12.95 kN, the crack further extended towards the loading zone, inducing severe propagation and instability.

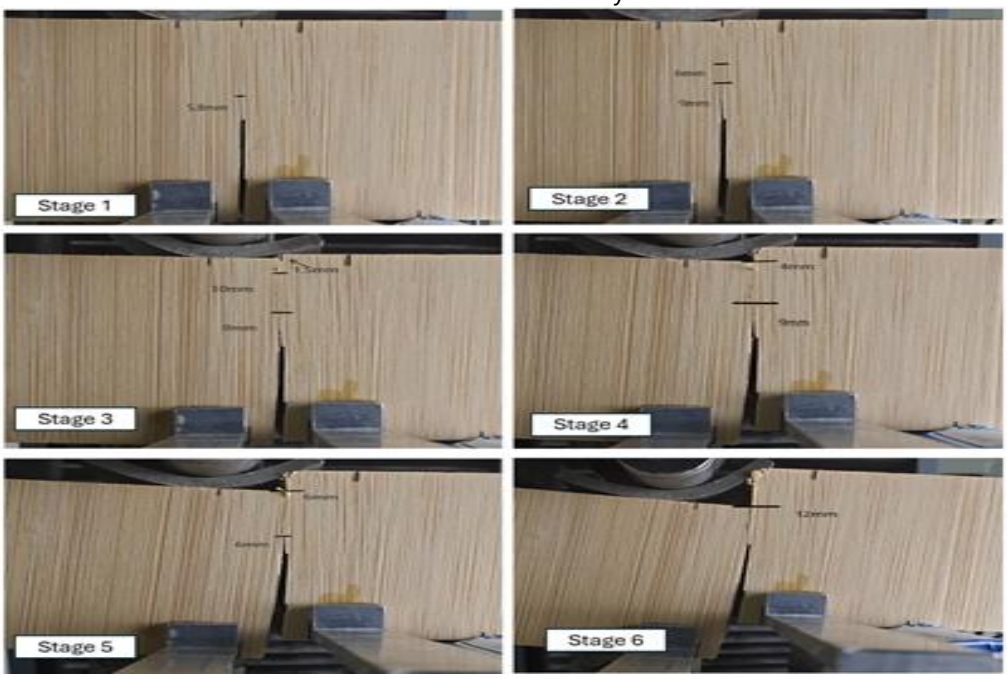

Figure 7:Fracture Stages of Group 1 ($0_2/90/0_2$, a/h = 0.5)

Table 3: fracture process for Group 3 ($90_2/0/90_2$, a/h = 0.5)

Stage	Time (s)	Load (kN)	Displacement (mm)	CMOD (mm)	CMSD (mm)	Crack Description
Stage 1	196	6.48	1.63	0.312	0.254	No visible change
Stage 2	409	11.41	3.4	0.582	0.935	Horizontal crack growth ~8.5 mm
Stage 3	797	14.72	6.64	1.429	5.394	Crack extended ~18 mm horizontally
Stage 4	1446	18.06	12.05	4.716	11.086	Inclined upward crack near loading point, large displacement
Stage 5	1718	15.89	14.32	5.292	11.077	Downward crack propagation ~12.5 mm, secondary crack ~9 mm
Stage 6	1961	12.95	16.34	5.288	11.076	Crack extended further toward loading point, severe propagation

Fracture process for Group 5 ($(0/90)_2/0$, a/h = 0.5)

The Group 5 fracture process developed progressively in a series of stages (Figure 9, Table 4). Around 353 s under a load of 9.87 kN, preliminary fine cracking noises were observed though fine cracks alone were visible with no apparent surface breakage. At 471 s when the load increased to 12.09 kN, cracks were seen and extended horizontally to around 9.2 mm, indicating the commencement of extensive fracture activity. At 532 s, under a load of 10.1 kN, there was greater distinct displacement on the left bamboo plate with 2.1 mm downward displacement, and the centre crack spread out to approximately 8.2 mm. Under continued loading, at 709 s (11.03 kN), extended crack propagation was observed with 3.8 mm downward displacement on the left plate, and the centre crack became compressed into a more slender, extended shape. By 1081 s, with a value below 12.19 kN, there was continuous crackling, and several fibre ruptures were evident in the central region, with CMOD and CMSD increasing sharply. At 1174 s, when the load decreased to 5.73 kN, the downward displacement

of the left plate increased, and the crack had progressed to an advanced stage of propagation. Lastly, the sequence suggested a progressive development of microcracks into a macrofracture, with Group 5 producing a relatively progressive yet unstable mode of fracture when compared to other geometries.

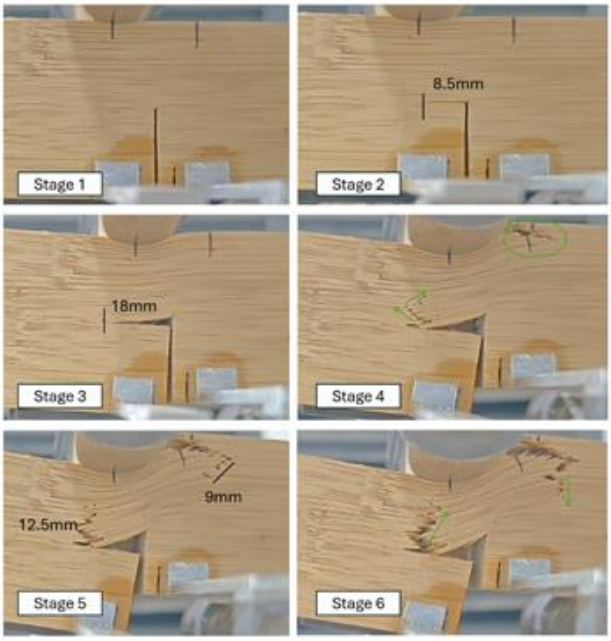

Figure 8: fracture process for Group 3 ($90_2/0/90_2$, a/h = 0.5)

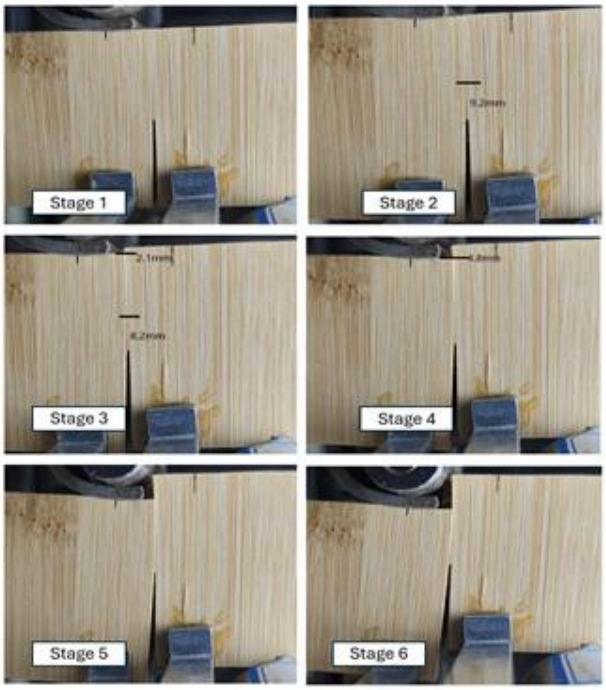

Figure 9:Fracture process for Group 5 ($(0/90)_2/0$, a/h = 0.5)

Table 4:Fracture process for Group 5 ($(0/90)_2/0$, a/h = 0.5)

Stage	Time (s)	Load (kN)	Displacement (mm)	CMOD (mm)	CMSD (mm)	Crack/Failure Description
1	353	9.87	2.94	0.939	0.141	First faint cracking sound; fine cracks appear, no obvious fracture visible.
2	471	12.09	3.93	1.25	0.056	Clear cracking sound; small cracks visible, extending horizontally to ~9.2 mm.
3	532	10.1	4.43	1.407	0.942	Continuous cracking; left plate displaces downward ~2.1 mm, central crack widens (~8.2 mm).
4	709	11.03	5.91	2.059	2.504	Further cracking; the left plate displaces downward by ~3.8 mm, with the central crack becoming compressed and elongated.
5	1081	12.19	9	3.396	5.566	Continuous crackling; more fibres are exposed in the middle region, and crack propagation accelerates.
6	1174	5.73	9.78	4.665	7.53	The left plate displaces downward significantly; this is an advanced stage of crack propagation leading to instability.

Fracture process for Group 7 ($(90/0)_2/90$, a/h = 0.5)

The Group 5 fracture process developed progressively in a series of stages Table 5,Figure 10. At a load of 9.87 kN, preliminary fine cracking noises were observed, although fine cracks alone were visible, with no apparent surface breakage. At 471 s, when the load increased to 12.09 kN, cracks were seen and extended horizontally to around 9.2 mm, indicating the commencement of extensive fracture activity. At 532 s, under a load of 10.1 kN, there was greater distinct displacement on the left bamboo plate with 2.1 mm downward displacement, and the centre crack spread out to approximately 8.2 mm. Under continued loading, at 709 s (11.03 kN), extended crack propagation was observed with 3.8 mm downward displacement on the left plate, and the centre crack became compressed into a more slender, extended shape. By 1081 s, with a value below 12.19 kN, continuous crackling was observed,

and several fibre ruptures were evident in the central region, with CMOD and CMSD increasing sharply. At 1174 s, when the load decreased to 5.73 kN, the downward displacement of the left plate increased, and the crack had progressed to an advanced stage of propagation. Lastly, the sequence suggested a progressive development of microcracks into a macrofracture, with Group 5 producing a relatively progressive yet unstable mode of fracture when compared to other geometries.

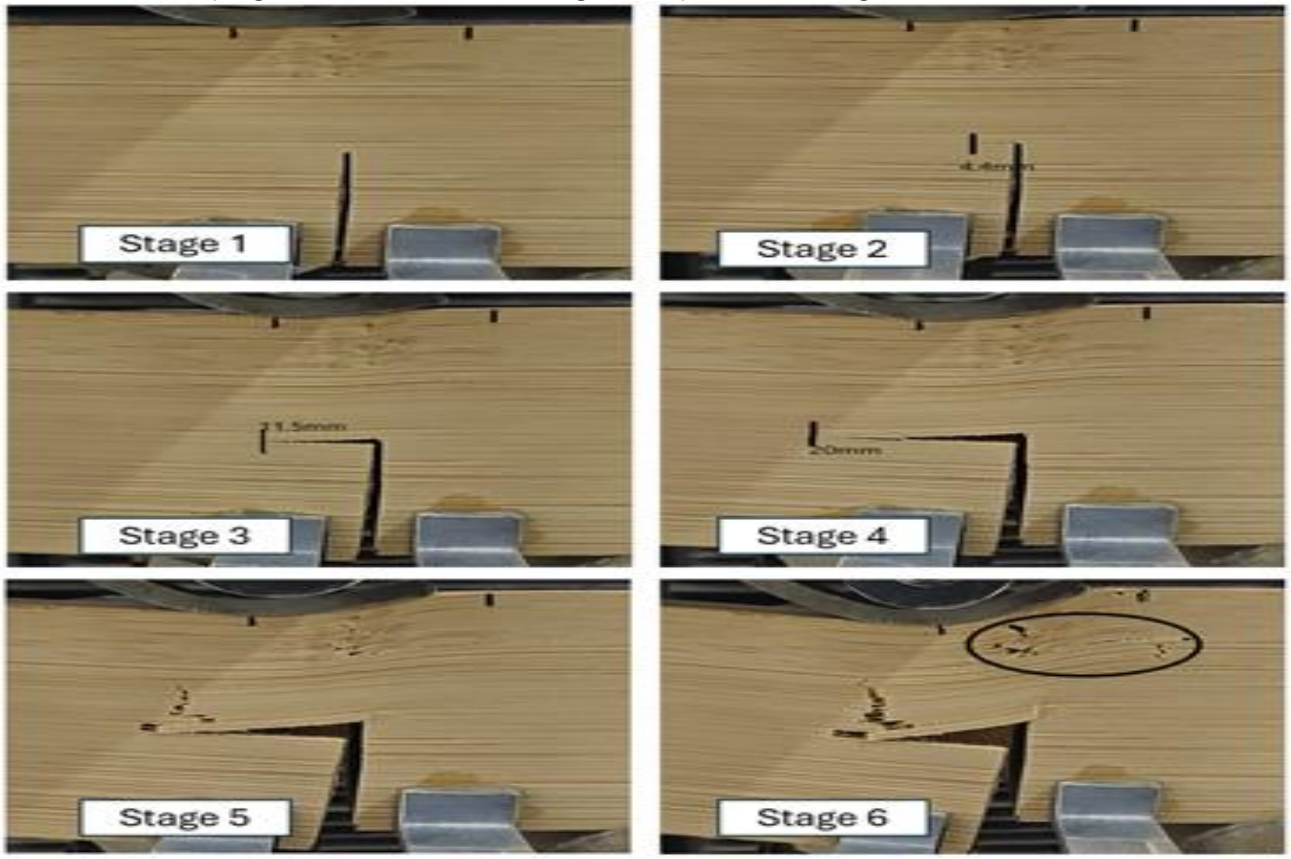

Figure 10: Fracture process for Group 7 ($(90/0)_2/90$, a/h = 0.5)

Table 5: Fracture process for Group 7 ($(90/0)_2/90$, a/h = 0.5)

Stage	Time (s)	Load (kN)	Displacement (mm)	CMOD (mm)	CMSD (mm)	Crack Description
Stage 1	257	7.8	2.14	0.478	0.153	No crack sound, no visible cracks
Stage 2	388	11.31	3.23	0.772	0.516	Faint cracking sound, small horizontal crack (~4.4 mm)
Stage 3	576	13.94	4.8	1.362	1.789	Weak crackling, crack extended horizontally (~11.5 mm), deformation starts.
Stage 4	783	16.36	6.53	2.222	3.165	Pronounced cracking, crack propagated horizontally (~20 mm)
Stage 5	984	16.51	8.2	3.839	5.541	Continuous cracking, diagonal upward propagation (~8.2 mm), fibre splitting
Stage 6	1206	13.26	10.05	5.996	8.694	Cracks expanded diagonally upward left, new cracks on the right (~10.05 mm)

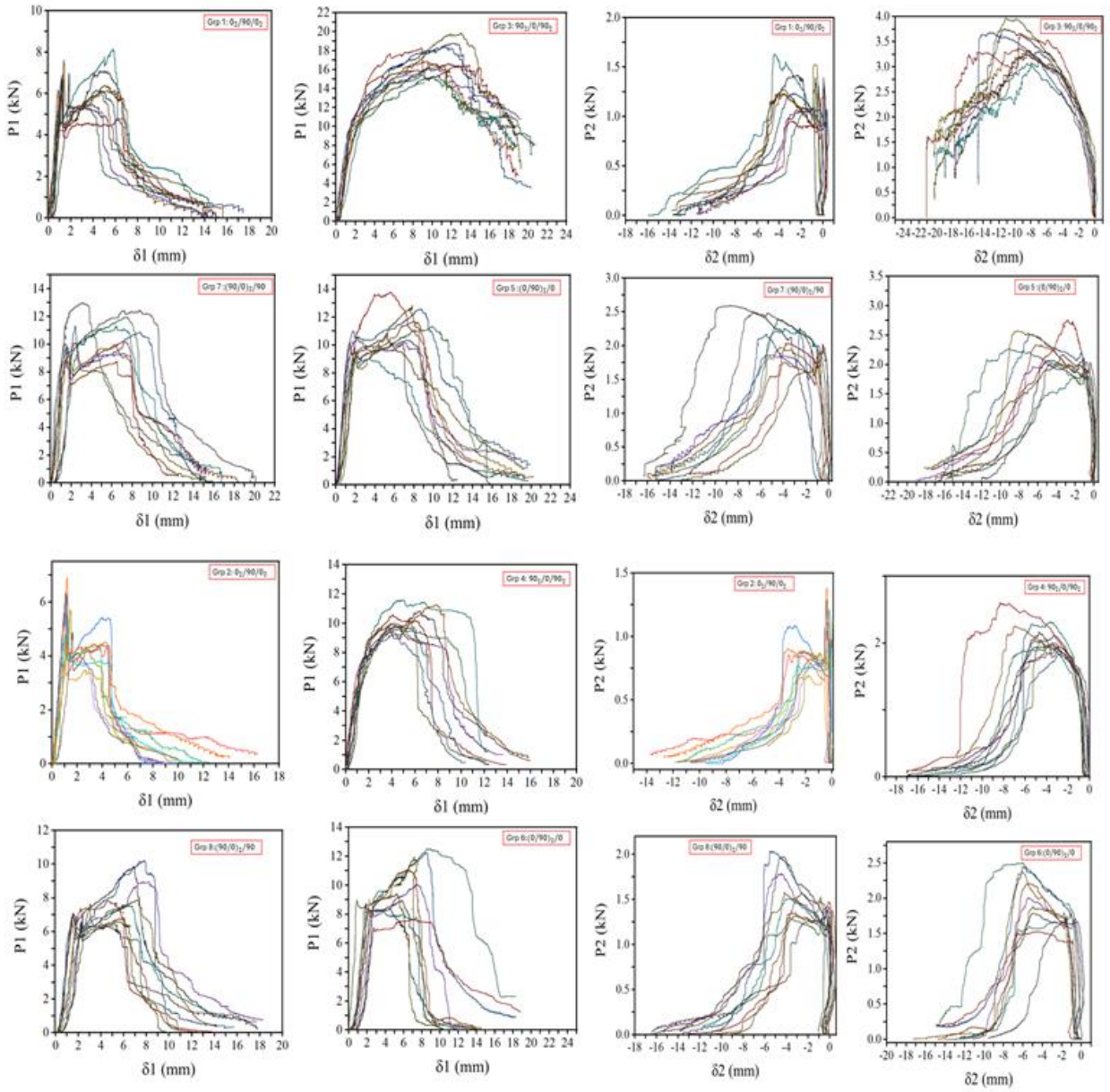

IV. RESULTS AND DISCUSSION

Analysis and Comparison of Groups with Initial Depth Ratio 0.5

The results of the four-point shear bending (FSB) test of Groups 1, 3, 5, and 7 with an initial depth ratio of 0.5 Table 6 They were compared to identify differences in the mechanical properties and fracture toughness. These groups showed different responses in terms of initial stiffness, load-carrying capacity, fracture toughness, and failure displacement, which are essential to evaluate their suitability for structural use. The initial stiffness values show that there are significant differences in deformation resistance between the groups. Group 3 had the highest initial load (18.95 kN) and displacement (12.037 mm), revealing that it is the most resistant to deformation among the groups. It has such high stiffness because the structure $90_2/0/90_2$ has a higher percentage of 90° layers, which enhances bending and shear resistance under loading. In contrast, Group 1 and Group 5 were less stiff, with Group 5 being the least stiff (load 3.25 kN, displacement 1.444 mm), while Group 7 was

moderately stiff (load 8.12 kN, displacement 2.387 mm) [33, 34]. Although Group 5 recorded a high maximum load (14.523 kN) and moderate displacement (5.27 mm), its performance was inferior to Group 3. While Group 3 displayed a smaller maximum load (6.085 kN) with minimal CMOD (0.179 mm) and CMSD (0.122 mm), its higher stiffness and capacity to resist deformation early in loading indicate superior performance in stiffness-dependent applications. The widespread presence of 90° orientations in Group 3's configuration explains these results, as these laminates are designed to improve stiffness and load distribution [35, 36]. Group 7 exhibited the highest peak load displacement (8.094 mm), reflecting greater flexibility and potential for energy absorption. However, its high CMSD value (4.981 mm) indicates excessive shear displacement, which could compromise its structural reliability in shear-critical conditions. While Group 5 showed equal CMOD and CMSD at failure, it remained below the initial resistance of Group 3. These findings clearly suggest that Group 3 possesses superior stiffness and early crack resistance, whereas the other groups tend toward flexibility and energy absorption [37, 38]. The analysis of crack mouth opening displacement (CMOD) and crack mouth slip displacement (CMSD) reveals further differences. Group 1 experienced moderate CMOD (1.258 mm) and CMSD (1.233 mm) at maximum load, indicating fair cracking resistance. Group 7, with its high displacement potential, exhibited very high CMSD values, reflecting a high propensity for shear slippage. Conversely, the relatively low CMOD and CMSD values in Group 3 suggest it effectively resists crack opening and shear displacement failures, consistent with the stabilising role of its 90° layers under load [39, 40]. Based on load, displacement, CMOD, and CMSD analyses, Group 3 appears to be the best performing configuration for a 0.5 depth ratio. Its enhanced initial stiffness and deformation resistance are linked to the increased content of 90° layers, which provide effective load distribution. While Groups 5 and 7 are more ductile and better at energy absorption, they are less suitable for applications prioritising initial stiffness and early crack resistance. Therefore, Group 3 stands out as the most reliable choice for structural applications requiring high stiffness and load-carrying capacity.

Table 6:the values of Load, displacement, CMOD, CMSD for the initial stifness and the maximum point

Group	Initial Stiffness			
	Load (kN)	Displacement (mm)	CMOD (mm)	CMSD (mm)
Grp 1	2.471	1.0752	0.652	0.413
Grp 3	18.95	12.037	4.931	11.935
Grp 5	3.25	1.444	4.931	0.086
Grp 7	8.12	2.387	0.459	0.229
Group	Max Point			
	Load (kN)	Displacement (mm)	CMOD (mm)	CMSD (mm)
Grp 1	8.2725	3.1675	1.258	1.233
Grp 3	6.085	1.627	0.179	0.122
Grp 5	14.523	5.27	2.668	1.593
Grp 7	8.15	8.094	2.901	4.981

Results for Groups with Initial Depth Ratio 0.6

For the 0.6 ratio groups (Grp 2, Grp 4, Grp 6, and Grp 8), the results of the four-point shear bending test show apparent differences in the stiffness, load capacity, and fracture behaviour parameters Table 7. While Grp 4 had the most stable crack resistance with very low CMOD (0.091 mm) and CMSD (0.138 mm), suggesting superior control of crack initiation and sliding at initial loading, Grp 6 was found to have the maximum resistance during the initial stiffness phase under 5.65 kN load and 1.84 mm displacement. Conversely, Grp 2 showed lowest stiffness (4.73 kN, 1.19 mm displacement) and confirmed its comparatively brittle nature.

At the state of maximum load, the optimum performance of Grp 4 can be observed. With notable crack opening (CMOD = 4.20 mm) and shear sliding (CMSD = 11.09 mm), it recorded a maximum load of 13.77 kN at a displacement of 11.9 mm. This mix exhibits good toughness and energy absorption by withstanding both extreme loads and deformations. Despite having the most significant displacement (12.4 mm) and absolute peak load (18.23 kN), Grp 8's more severe CMOD and CMSD indicate less stability of crack growth than Grp 4. Grp 2 was once again the

worst (6.76 kN, 2.95 mm), while Grp 6 was equally good (12.75 kN, 9.02 mm) despite having a lower displacement capacity. Grp 4 has the higher load-carrying capacity, crack resistance, stability, and controlled shear sliding, making it the ideal balanced composition, even though Grp 8 is generally the strongest. It is the most dependable of the 0.6 ratio groups for the use of structures where both strength and stability against a crack are factors, and its larger number of 90° layers also appears to be of primary importance in stress redistribution and an increase in fracture toughness.

Table 7: the values of Load, displacement, CMOD, CMSD for the initial stifness and the maximum point

Group	Initial Stiffness			
	Load (kN)	Displacement (mm)	CMOD (mm)	CMSD (mm)
Grp 2	4.725	1.195	0.424	0.2365
Grp 4	4.98	1.44	0.091	0.138
Grp 6	5.65	1.84	0.507	0.033
Grp 8	5.34	1.32	0.444	0.171
Group	Max Point			
	Load (kN)	Displacement (mm)	CMOD (mm)	CMSD (mm)
Grp 2	6.76	2.95	1.297	2.176
Grp 4	13.77	11.9	4.197	11.091
Grp 6	12.75	9.02	2.87	10.7
Grp 8	18.23	12.4	5.01	11.23

V. FRACTURE SURFACE OBSERVATION (SEM ANALYSIS)

After the macroscopic fracture process scanning of Groups 1, 3, 5, and 7 (notch ratio 0.5) in Figure 12, the fracture surfaces were subsequently examined using Scanning Electron Microscopy (SEM) to gain insightful information on microscale failure mechanisms of the fractures. SEM analysis is of particular importance to laminated composites such as bamboo because it reveals the interface of fibre morphology, matrix response, and interfacial adhesion that governs the fracture process and energy absorption [41, 43]. For Group 1 ($0_2/90/0_2$), SEM micrographs showed large fibre pull-out and matrix cracking with localised delamination between neighbouring laminae. These features show that the crack growth was not totally brittle but comprised sequential fibre–matrix debonding in series, which dissipated some energy. Such a response agrees with previous observations on laminated composites in which delamination controlled interfacial fracture under mixed-mode loading [44]. In contrast, Group 3 ($90_2/0/90_2$) with the highest initial macro-level stiffness showed very different fracture surface characteristics. SEM micrographs revealed brittle fibre failure with relatively smooth fracture surfaces and little fibre pull-out evidence.

This confirms the observation that the high-stiffness configuration constrained micro-level energy dissipation and promoted catastrophic brittle failure upon cracking.. Similar fracture surfaces with extensive fibre breakage have also been reported for high-density unidirectional laminates with a predominance of the transverse layer [45, 46]. Group 5 ($(0/90)_2/0$) displayed a more complex fracture morphology. SEM observations showed fibre bridging, shear hackles, and localised matrix shearing, all indicative of increased resistance to crack growth. Fibre bridging, in particular, acts as an alleviation mechanism that transfers stress along the crack front and delays the unstable propagation of the crack. [47].

The occurrence of shear hackles further indicates extensive shear-dominated crack growth and suggests that this arrangement absorbed more fracture energy than Grps 1 and 3. Lastly, Grp 7 ($(90/0)_2/90$) displayed a mixed mode of fracture. SEM images revealed interfacial debonding regions as well as high fibre pull-out levels, in addition to localised brittle fracture of the fibres. The bimodal response aligns with the macroscopic observation, where the samples were more tolerant to displacement but experienced over-shearing deformation. The hybrid fracture pattern further suggests a competition between fibre bridging and interfacial failure mechanisms, both of which have been seen in alternating layer orientation laminated composites [48, 49]. Overall, these microscopically obtained findings are in strong agreement with the macroscopic fracture test results, and these also

support the fact that the layer orientation (0° vs. 90°) plays a pivotal role in deciding whether the fracture response will be brittle or ductile. 90° layer-dominated layups (e.g., Grp 3) are predisposed toward stiffness but brittle failure. In contrast, alternating or mixed orientations (e.g., Groups 5 and 7) favour mechanisms such as fibre pull-out and bridging, leading to enhanced fracture toughness and energy absorption. This synergy between the layer orientation and microscale fracture mechanisms highlights the importance of optimum design of laminate in bamboo composites for targeted structural application [50, 52]

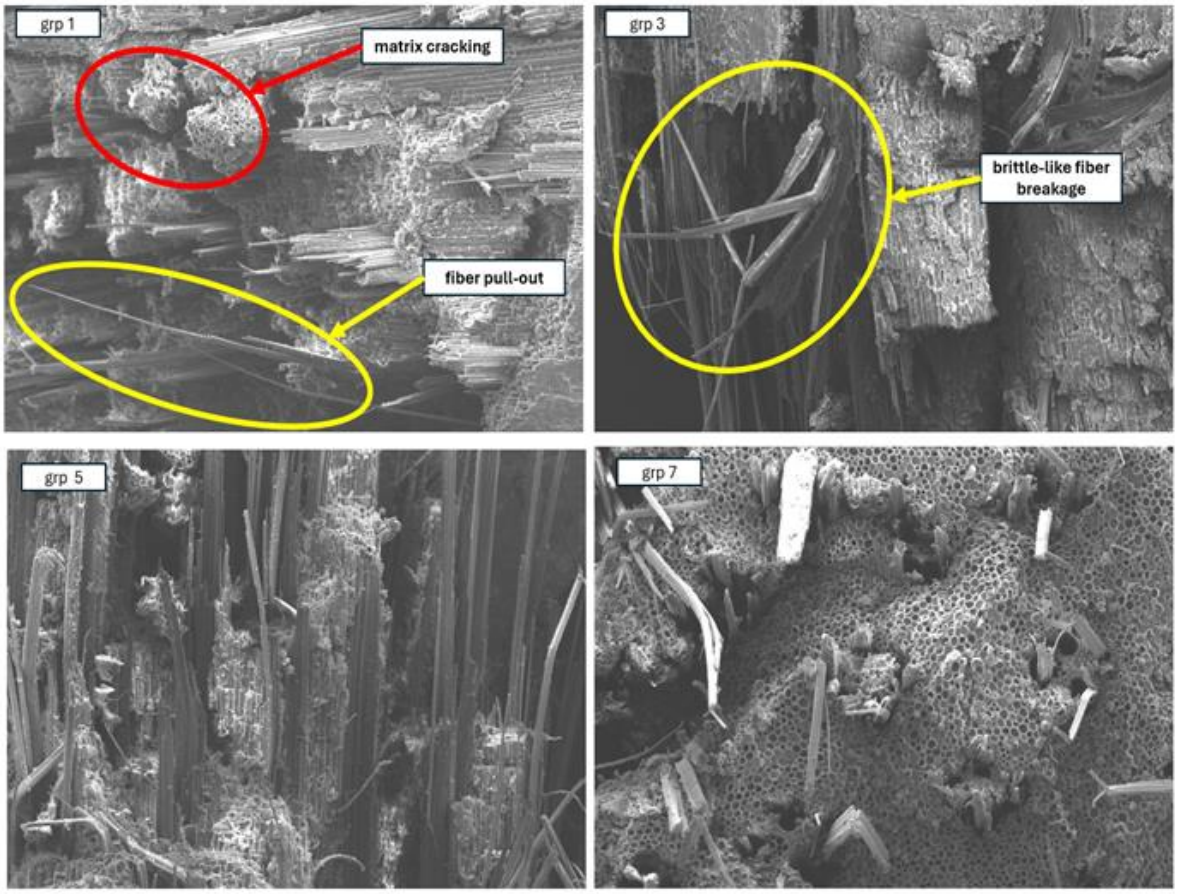

VI. CONCLUSION

We have investigated the fracture behaviour of five-layer laminated bamboo beams under four-point shear bending with two initial notch-to-depth ratios (0.5 and 0.6). Eight specimen groups were tested experimentally to investigate the effects of fibre direction and notch ratio on mechanical performance, crack initiation, propagation, and ultimate failure. The results provided new data on the flexural behaviour, fracture process, and microstructural failure mechanisms of laminated bamboo. Different fracture types were observed in the notch ratio 0.5 groups. Group 1 ($0_2/90/0_2$) showed medium performance and failed due to low crack resistance and brittle fracture.

Group 3 ($90_2/0/90_2$) had the highest initial stiffness and load-carrying capacity, owing to its higher percentage of 90° orientation layers, but exhibited a more brittle failure mode with fibre breakage occurring close together but group 5 $(0/90)_2/0$ demonstrated the most symmetrical behaviour, with stable crack growth, fibre bridging, and higher energy absorption with respect to group 7 $(90/0)_2/90$ balanced moderate strength with considerable displacement tolerance, with failure involving delamination and shear sliding control. Overall, the strength and ductility were greater in the 0.6 notch ratio groups than in the 0.5 ratio groups. Group 2

was the weakest, failing catastrophically under low loads. Group 4 ($90_2/0/90_2$) displayed a favourable combination of peak load (13.77 kN), displacement (11.9 mm), and stable shear resistance, while Group 6 $(0/90)_2/0$ performed reasonably well but with greater variability while group 8 $(90/0)_2/90$ recorded the highest peak load (18.23 kN) and displacement (12.4 mm), though with less stable crack propagation surfaces compared to Group 4.

Fracture process analysis revealed that failure in laminated bamboo occurs in three stages: crack initiation at the notch, stable propagation through fibre debonding and delamination, and ultimately, an unstable catastrophic fracture dominated by fibre rupture and shear sliding. Correlation of fracture stages with load–CMOD, load–displacement, and load–CMSD curves indicated that larger ratios of 90° layers delayed unstable fractures and improved stiffness but at the cost of ductility. SEM analysis corroborated these microstructural findings: Group 1 exhibited matrix cracking and fibre pull-out, which typifies delamination-controlled failure; Group 3 showed brittle fibre fracture characteristic of its stiff but brittle macroscopic behaviour; Group 5 displayed energy-absorbing shear hackles and bridging fibres; and Group 7 exhibited multi-mode fracture, including interfacial debonding and fibre pull-out.

These microstructural tests determined the effect of lay-up orientation on fracture toughness and highlighted the importance of fibre–matrix interaction in the behaviour of bamboo. Overall, the research indicates that the notch ratio and laminate orientation significantly influence the fracture resistance of laminated bamboo. Layers oriented at 90° (Groups 3 and 4) offered better stiffness and load-carrying capacity, whereas mixed orientations (Groups 5 and 7) enhanced fracture toughness and energy absorption.

Among the tested groups, Groups 4 ($90_2/0/90_2$, a/h = 0.6) and 5 ($(0/90)_2/0$, a/h = 0.5) are recommended as optimal designs, as they provide a favourable combination of strength, toughness, and crack stability. These findings not only deepen the understanding of laminated bamboo fracture mechanics but also facilitate the development of optimised designs for sustainable structural applications.

Authors

- **Yassine Dahbi:** Main author of the paper; responsible for conceptualisation, methodology, conducting experiments, data analysis, and writing the initial draft.
- **Yao Wu:** Supervisor; provided overall guidance and supervision of the research process.
- **Huang Xuejian:** Assisted with experimental work, specimen preparation, and data processing.
- **Hamza Zaouri:** Contributed to manuscript editing, refining the writing, and providing support to the research team.

REFERENCES

1. Liese, W., & Kumar, S. (2003). Bamboo as a building material: Properties and processing. In S. S. K. Ghimire & B. H. B. Chakraborty (Eds.), Bamboo: The versatile material for the future. FAO.
2. Silva, J. A., & Rodrigues, P. L. (2021). Bamboo as a sustainable resource for construction and building industries: A review. Journal of Renewable and Sustainable Energy, 13(2), 210-226. https://doi.org/10.1063/5.0045358
3. Hadi, H., & Fadaei, F. (2016). Mechanical properties of laminated bamboo: Strength and durability characteristics. Construction and Building Materials, 123, 236-245. https://doi.org/10.1016/j.conbuildmat.2016.07.128
4. Pradhan, S. K., & Kumar, S. (2015). Effect of bamboo laminate orientation on flexural strength: Experimental investigation. Materials and Design, 66, 145-153. https://doi.org/10.1016/j.matdes.2014.10.073
5. Chandrasekaran, M., & Jayaraman, K. (2017). Structural performance of laminated bamboo under flexural loading. Composites Part B: Engineering, 108, 121-131. https://doi.org/10.1016/j.compositesb.2016.09.039

6. Soni, P., & Gupta, A. (2020). Laminated bamboo in sustainable architecture: A review of applications and performance. Journal of Green Building, 15(2), 69-84. https://doi.org/10.3992/1943-4618.15.2.69
7. Ferreira, A., & Fernandes, P. (2019). Bamboo as a structural material in modern construction: A case study of laminated bamboo beams. Construction and Building Materials, 215, 369-377. https://doi.org/10.1016/j.conbuildmat.2019.04.034
8. Li, X., & Wu, Z. (2019). Bamboo in construction: From ancient wisdom to modern-day applications. Sustainable Materials and Technologies, 21, e00107. https://doi.org/10.1016/j.susmat.2019.e00107
9. Xu, Z., & Xu, Z. (2018). Bamboo forests and carbon sequestration: How bamboo can mitigate climate change. Environmental Science & Policy, 87, 59-69. https://doi.org/10.1016/j.envsci.2018.05.002
10. Pandey, D. (2020). Carbon storage potential of bamboo: A global perspective. Environmental Management and Sustainability, 7(3), 112-124. https://doi.org/10.1007/s12640-020-00204-0
11. Bahrami, B., et al. (2020). Effect of support conditions on fracture toughness testing. Engineering Fracture Mechanics, 234, 107139.
12. Ayatollahi, M., et al. (2019). Support friction and its influence on fracture behavior. International Journal of Solids and Structures, 162, 199-210.
13. Wang, X., et al. (2018). Influence of boundary conditions on fracture behavior of laminated composites. Composite Structures, 200, 112-121.
14. Dong, C., et al. (2020). Methodology for analyzing fracture test data in bamboo and composites. Construction and Building Materials, 261, 120506.
15. Sharma, B., Gatóo, A., Bock, M., & Ramage, M. (2015). Engineered bamboo for structural applications. Construction and Building Materials, 81, 66–73.
16. Sharma, B., & Ramage, M. H. (2017). The potential of engineered bamboo in sustainable construction. Journal of Materials Research, 32(19), 3431–3442.
17. Nugroho, N., & Ando, N. (2001). Development of structural composite products made from bamboo II: Fundamental properties of laminated bamboo board. Journal of Wood Science, 47, 237–242.
18. Amada, S., & Untao, S. (2001). Fracture properties of bamboo. Composites Part B: Engineering, 32(5), 451–459.
19. Yu, W., Jiang, Z., & Li, X. (2014). Fracture mechanics of bamboo with different loading directions. Wood Science and Technology, 48, 1171–1181.
20. Ghavami, K. (2005). Bamboo as reinforcement in structural concrete elements. Cement & Concrete Composites, 27(6), 637–649.
21. Kaminski, S., Lawrence, A., & Trujillo, D. (2016). Structural use of bamboo: Part 1 – Introduction to bamboo. The Structural Engineer, 94(8), 40–47.
22. Kaminski, S., Trujillo, D., & Lawrence, A. (2016). Structural use of bamboo: Part 2 – Design codes and applications. The Structural Engineer, 94(9), 52–58.
23. Xiao, Y., & Yang, R. (2012). Design and application of laminated bamboo lumber. Journal of Materials in Civil Engineering, 24(10), 1390–1397.
24. Li, X., & Shen, Y. (2011). Mechanical behavior of laminated bamboo under bending and compression. Construction and Building Materials, 25(6), 2640–2649.
25. Huang, D., Zhou, A., & Bian, Y. (2013). Experimental and analytical study on mechanical properties of parallel strand bamboo. Construction and Building Materials, 38, 627–632.
26. Correal, J. F., & Echeverry, J. S. (2014). Mechanical properties of Colombian glued laminated bamboo. Construction and Building Materials, 72, 105–112.
27. Chaowana, K. (2013). Bamboo: An alternative raw material for wood and wood-based composites. Journal of Materials Science Research, 2(2), 90–102.
28. Yu, Y., Zhu, R., Wu, B., & Yu, W. (2011). Comparative analysis of the mechanical properties of bamboo and wood. European

Journal of Wood and Wood Products, 69, 509–513.
29. Li, H., Wu, G., & Wang, Z. (2015). Evaluation of laminated bamboo as a structural material. BioResources, 10(3), 6002–6015.
30. Hidalgo-López, O. (2003). Bamboo: The Gift of the Gods. Bogotá: D'VINNI Ltda.
31. Lakkad, S. C., & Patel, J. M. (1981). Mechanical properties of bamboo, a natural composite. Fiber Science and Technology, 14(4), 319–322.
32. Dixon, P. G., & Gibson, L. J. (2014). The structure and mechanics of moso bamboo material. Journal of the Royal Society Interface, 11(99), 20140321.
33. Obataya, E., & Norimoto, M. (1999). Moisture-dependent changes in dynamic viscoelastic properties of bamboo. Journal of Wood Science, 45, 337–342.
34. Nogata, F., & Takahashi, H. (1995). Intelligent functionally graded material: Bamboo. Composites Engineering, 5(7), 743–751.
35. Ray, A. K., Mondal, S., Das, S. K., & Ramachandra, R. S. (2005). Study of the mechanical behavior of bamboo. Journal of Materials Science, 40, 5249–5256.
36. Scurlock, J. M. O., Dayton, D. C., & Hames, B. (2000). Bamboo: An overlooked biomass resource? Biomass and Bioenergy, 19(4), 229–244.
37. Ghavami, K., & Marinho, A. B. (2005). Experiments on the mechanics of bamboo materials. Materials Research, 8(3), 259–268.
38. Lee, A. W. C., Bai, X., & Bangi, A. P. (1994). Selected physical and mechanical properties of giant timber bamboo grown in South Carolina. Forest Products Journal, 44(9), 40–46.
39. Li, H., & Shen, L. (2019). Micromechanical characterization of bamboo fibers and their interfacial behavior in composites. Composites Part A: Applied Science and Manufacturing, 125, 105563.
40. Tan, T., Liu, H., & Jiang, Z. (2018). Fracture and energy absorption mechanisms of natural fiber composites under different loading conditions. Composites Science and Technology, 162, 106–115.
41. Wang, Z., Yu, Y., & Zhu, R. (2017). Fracture toughness of unidirectional laminated bamboo composites. Journal of Materials Science, 52, 4590–4603.
42. Hu, C., Wang, G., & Xie, Y. (2020). Brittle and ductile fracture behavior in laminated composites under mode I loading. Theoretical and Applied Fracture Mechanics, 108, 102629.
43. Ashby, M. F., & Gibson, L. J. (1997). Cellular Solids: Structure and Properties. Cambridge University Press.
44. Silva, J. F., & Rodrigues, A. (2021). Failure analysis of natural fiber composites: mechanisms and fracture morphologies. Composite Structures, 261, 113284.
45. Ferreira, J. A. M., & Fernandes, J. V. (2017). Mixed-mode fracture in laminated composites: experimental observations and failure mechanisms. International Journal of Solids and Structures, 118–119, 50–61.
46. Li, H., Wu, G., & Zhang, Q. (2016). Microstructural characteristics and mechanical performance of laminated bamboo under flexural loading. Construction and Building Materials, 123, 58–65.
47. Pradhan, S., & Kumar, A. (2020). Flexural and fracture properties of engineered bamboo laminates with different fiber orientations. Journal of Renewable Materials, 8(5), 569–582.
48. Soni, R., & Gupta, A. (2021). Fracture and failure mechanisms of laminated bamboo composites under axial and bending loads. Materials Today: Proceedings, 44, 2314–2321.
49. Sharma, B., et al. (2014). Engineered bamboo: State of the art. Proceedings of the Institution of Civil Engineers – Construction Materials, 167(3), 152–161.
50. Trujillo, D., & Lo, T. Y. (2016). Mechanical properties of bamboo and bamboo composites: A review. Construction and Building Materials, 127, 727–740.
51. Wei, Y., & Jiang, Z. (2020). Microstructural analysis and fracture behavior of laminated bamboo composites under flexural stress. Composite Structures, 235, 111788.
52. Zhou, A., Huang, D., & Bian, Y. (2012). Experimental study on the flexural behavior of laminated bamboo beams. Construction and Building Materials, 29, 334–341.